Stability of tantalum-doped $Li_7La_3Zr_2O_{12}$ (LLZO) via cluster expansion and Monte Carlo

Kemeridge Malatji*, *Refiloe* Maphoto, *Malang* Masedi, *Phuti* Ngoepe, and *Raesibe* Ledwaba

Materials Modelling Centre, University of the Limpopo, South Africa
Kemeridge.malatji@ul.ac.za, refiloekhomotso@gmail.com, cliffton.masedi@ul.ac.za, phuti.ngoepe@ul.ac.za, raesibe.ledwaba@ul.ac.za

Abstract. This study employs first-principles calculations and cluster expansion to explore new stable phases of Ta-doped LLZO ($Li_5La_3Zr_{2-x}Ta_xO_{12}$) to enhance the conductivity of the tetragonal structure. Monte Carlo simulations further analyze the temperature-dependent behavior of these phases under the canonical ensemble and determine phase transition of mixed systems. The structures were selected by identifying those with the lowest energy at various compositions from the cluster expansion, where the low cross-validation score (CVS < 5 meV) guarantees the predicted energies are highly accurate and physically meaningful, allowing for a reliable assessment of thermodynamic stability. The structures were selected by identifying those with the lowest energy at various compositions from the cluster expansion. The cluster expansion reveals 28 miscible multi-component structures, all thermodynamically stable with negative formation enthalpies. Monte Carlo results indicate no phase separation, with optimal mixing at ~900 K. These findings suggest Ta doping improves structural stability without compromising miscibility, offering potential pathways for higher ionic conductivity.

1 Introduction

The rapid advancement of new energy technologies has driven increasing demand for lithium-ion batteries that combine high energy density with exceptional safety. Solid-state lithium-ion batteries (SSLIBs) have emerged as particularly promising candidates for next-generation energy storage, offering potential applications in mobile electronics and electric vehicles while addressing safety concerns associated with conventional liquid electrolytes [1-3]. Among solid-state electrolytes (SSEs), oxide-garnet structured $LiLa_3Zr_2O_{12}$ (LLZO) has attracted significant attention due to its remarkable ionic conductivity (~10^{-3} S cm^{-1}), excellent electrochemical stability with lithium metal, and superior safety characteristics [4,5]. However, the room-temperature stabilization of LLZO in its highly conductive cubic phase remains challenging, as the material naturally crystallizes into a less conductive tetragonal (t-LLZO) phase under ambient conditions. Doping strategies have proven effective

* Corresponding author: kemeridge.malatji@ul.ac.za

in modifying LLZO's phase stability and ionic conductivity. Supervalent cation substitution, particularly at the Zr-site, has demonstrated significant potential for stabilizing the tetragonal phase while enhancing ionic conductivity through controlled lithium vacancy creation [6-9]. For instance, Al^{3+} and Ga^{3+} doping at Li sites has been shown to stabilize the cubic phase and improve conductivity [10-12], with optimal Al doping concentrations (0.2-0.24 mol) yielding particularly promising results [13,14]. However, Zr-site doping offers distinct advantages, as the (0, 0, 0) Wyckoff position and fully ordered Li sites provide a more straightforward framework for systematic modification. Ta^{5+} doping at Zr^{4+} sites have emerged as a particularly promising approach, as it not only stabilizes the tetragonal structure but also activates previously inaccessible Li^{+} conduction pathways [15].

Despite these advances, significant challenges remain in understanding the high-temperature phase behaviour of doped LLZO and optimizing its ionic conductivity at room temperature. Traditional materials development approaches often involve time-consuming trial-and-error processes [16], highlighting the need for more efficient predictive methods. Cluster expansion techniques, particularly when combined with first-principles calculations, offer a powerful alternative by enabling systematic exploration of configurational space and accurate prediction of material properties [17]. The MedeA-Universal Cluster Expansion (UNCLE) code implements this approach through genetic algorithm optimization, facilitating efficient ground-state searches and thermodynamic simulations [18].

Combining first-principles density functional theory (DFT) with cluster expansion, we map the phase stability of Ta-doped tetragonal LLZO. A genetic algorithm-based ground-state search reveals novel, thermodynamically stable compositions that exhibit superior ionic conductivity. Complementary Monte Carlo simulations under canonical ensemble conditions provide insights into the temperature-dependent behaviour of these doped phases, offering a comprehensive understanding of their thermodynamic stability and potential for practical applications.

2 Methodology

The configurational thermodynamics of tetragonal LLZO (t-LLZO) were investigated using a Cluster Expansion (CE) approach, as implemented in the MedeA-Universal Cluster Expansion (UNCLE) package [16]. Starting from the geometrically optimized t-LLZO crystal structure, we used UNCLE to automatically generate and converge a CE Hamiltonian. This method systematically identifies the unique clusters from pairs to multi-body interactions—that are essential for describing the energy of configurations within the random mixing regime. A set of effective cluster interactions (ECIs) is extracted from a cluster expansion that has been optimized via fitting to first-principles data and regularization to prevent overfitting and is subsequently used in large-scale Monte Carlo simulations to predict thermodynamic properties. We employed a multi-scale computational approach to investigate the stability and properties of Ta-doped LLZO. First, Monte Carlo (MC) simulations were performed using the UNCLE package to sample configurations across different temperatures and concentrations. These simulations utilized a 5×5×5 supercell (~11,000 atoms) within the canonical (NVT) ensemble. Subsequently, the most stable configurations identified from the MC sampling were selected for ab initio density functional theory (DFT) calculations. These calculations were executed within the MedeA software environment [17] using the VASP code. The electron-ion interaction was described by projector-augmented wave (PAW) potentials [18], and the exchange-correlation functional was treated with the Perdew-Burke-Ernzerhof (PBE) generalized-gradient approximation (GGA). A plane-wave kinetic energy cutoff of 500 eV and a 5×5×1 Monkhorst-Pack k-point mesh were used for the structural optimization of the $Li_5La_3Zr_{2-x}Ta_xO_{12}$ supercells. Fermi-surface smearing was applied with the first Methfessel-Paxton method and a width of 0.2 eV

to accelerate convergence. The electronic self-consistent field cycle was converged to 10^{-5} eV, and ionic relaxation was considered complete when the forces on all atoms were below 0.01 eV/Å using a conjugate-gradient algorithm.

3 Results and discussion

The structural exploration of t-LLZO was performed using the MedeA-Universal Cluster Expansion (UNCLE) package [16], which enables automated construction and convergence of cluster expansions for complex systems. Starting from geometrically optimized t-LLZO structures, the package identified unique clusters within the random mixing regime and extracted a set of effective cluster interactions. These parameters were subsequently employed in large-scale Monte Carlo simulations using a 5×5×5 supercell (11,000 atoms) under canonical ensemble conditions across various temperatures and concentrations. This section presents a detailed analysis of: (1) the phase stability diagram derived from cluster expansion, (2) temperature-dependent Monte Carlo simulation profiles, and (3) the convergence behaviour of the ground-state search as characterized by cross-validation scores (CVS) and iteration analysis. Together, these results provide fundamental insights into the thermodynamic stability and temperature-dependent behaviour of the generated Ta-doped t-LLZO structures.

3.1 Phase stability diagram

Using a 1-unit cell model, we conducted a search for novel thermodynamically stable phases, which simplified both the CE ground-state search and DFT energy calculations by reducing the complexity inherent to the atomic arrangement in the LLZO garnet structure. Effective cluster interactions were determined through a genetic algorithm (GA) fitting scheme, implemented over a maximum of 23 iterations. The algorithm began with an initial training set of 20 structures and added up to 9 new structures per iteration, continuing until convergence was achieved (i.e., no further structures were predicted by the CE). As illustrated in Figure 1, panel (a) tracks the number of newly generated structures per iteration, while panel (b) monitors the corresponding cross-validation scores, serving to evaluate both the structural discovery rate and the accuracy of DFT energy predictions for the generated configurations.

The ground-state search was initiated using parent structures $Li_5La_3Zr_2O_{12}$ and $Li_5La_3Ta_2O_{12}$ (Iteration 0), followed by 20 randomly selected structures generated via the UNCLE code's genetic algorithm (Iteration 1). The optimal set of structures and their interaction parameters were iteratively refined using energies from the training set (Iterations 1–22). Convergence was achieved at Iteration 23, where zero new structures were generated (Figure 1a), confirming both the completion of the CE search and the accuracy of DFT energy evaluations. Cross-validation (CV) analysis assessed the reliability of the structures, with the CV score (CVS) serving as a metric for predictive accuracy. Initial iterations (1–9) yielded a stable CVS of 0.45 meV/atom, followed by fluctuations (peak: 0.48 meV/atom at Iteration 11; minimum: 0.18 meV/atom at Iteration 12). Beyond Iteration 12, the CVS remained below 0.46 meV/atom (Figure 1b), demonstrating improved DFT accuracy and robust generalization. All structures exhibited CVS values <5 meV/atom well within the threshold for reliable predictions, eliminating the need for standard deviation analysis and ensuring practical applicability without Monte Carlo sampling errors.

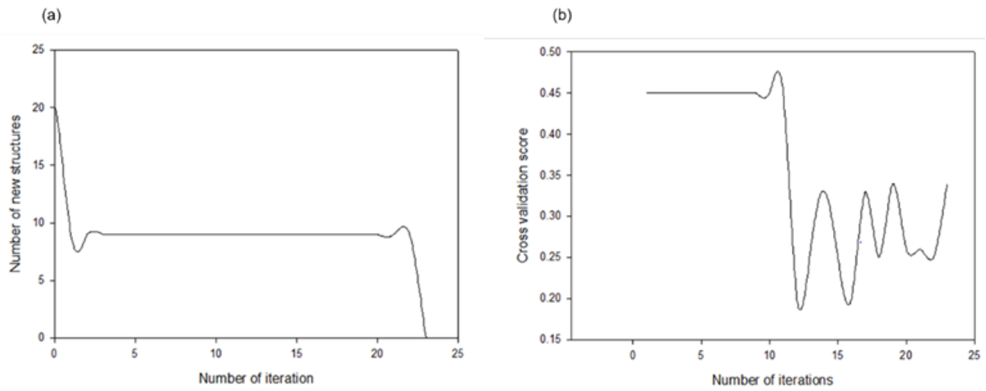

Fig. 1. Caption of the Figure 1. B (a) New ground-state structures versus the number of iterations, (b) cross-validation score versus number iterations.

Figure 2 shows the entropy of formation versus Ta concentration from cluster expansion (CE) calculations, along with the binary thermodynamic stability diagram (convex hull) that summarizes the stability of newly favourable phases. The diagram displays CE-predicted (green crosses) and DFT-calculated (green squares) enthalpies of formation for training set structures, along with CE-predicted enthalpies for other considered structures (grey crosses). The CE produced 28 new phases with varying Ta concentrations and symmetries, including the parent phases $Li_5La_3Zr_2O_{12}$ (x=0) and $Li_5La_3Ta_2O_{12}$ (x=1) on the solid black line. The ground-state line (red solid line) comprises structures with negative formation enthalpies, confirming their thermodynamic stability, while structures with positive enthalpies require external stabilization. Five particularly stable phases lie on this line: $Li_5La_3ZrTaO_{12}$ ($P\bar{1}$), $Li_5La_3Zr_{0.5}Ta_{1.5}O_{12}$ (C2/c), $Li_5La_3Zr_{1.5}Ta_{0.5}O_{12}$ ($P\bar{1}$), $Li_5La_3Zr_{1.75}Ta_{0.25}O_{12}$ ($P\bar{1}$), and $Li_5La_3Zr_{0.25}Ta_{1.75}O_{12}$ ($P\bar{1}$), demonstrating that Zr-site Ta doping yields energetically favourable configurations for solid electrolyte applications.

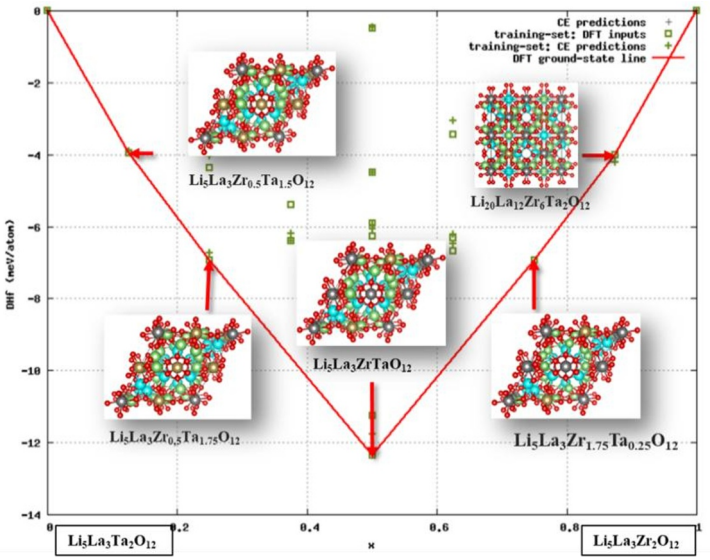

Fig. 2. Formation enthalpy (ΔH_f) vs. Ta content (x) in $Li_5La_3Zr_{2-x}Ta_xO_{12}$. Red line: DFT ground states; green: CE predictions.

3.2 Phase stability and critical temperature analysis via Monte Carlo simulation

To evaluate the phase stability of the $Li_5La_3Zr_{2-x}Ta_xO_{12}$ compounds, we employed large-scale Monte Carlo (MC) simulations based on a converged cluster expansion (CE). This approach leverages a set of effective cluster interactions to stochastically explore system configurations, sampling states with probabilities that reflect their true physical likelihood. The simulations were conducted within the canonical ensemble to explicitly study the phase separation behaviour as a function of temperature. Using a 5x5x5 supercell containing 11,000 atoms, we performed simulations from an initial temperature of 200 K up to a final temperature of 3000 K. Each simulation ran for a minimum of 300,000 steps to ensure proper sampling, with an energy convergence criterion set to 0.0001 Å. The concentration for each simulation was fixed to that of the most stable structures identified by the CE, allowing us to analyse the temperature-dependent behaviour at specific compositions. The resulting Monte Carlo temperature profiles are shown in Figures 3.1(a) and 3.2(b-c) for different Zr/Ta concentrations: (a) $Zr_{0.5}Ta_{0.5}$: Corresponding to the stable structure $Li_5La_3ZrTaO_{12}$ ($P\bar{1}$), (b) $Zr_{0.25}Ta_{0.75}$: Corresponding to $Li_5La_3Zr_{0.5}Ta_{1.5}O_{12}$ (C2/c), (c) $Zr_{0.125}Ta_{0.875}$: Corresponding to $Li_5La_3Zr_{0.25}Ta_{1.75}O_{12}$ ($P\bar{1}$). Analysis of these profiles reveals the critical temperature (T_c) at which atomic mixing occurs. For the $Zr_{0.5}Ta_{0.5}$ and $Zr_{0.125}Ta_{0.875}$compositions, this mixing transition occurs at approximately 800 K, accompanied by small energy differences of 0.9 eV/atom and 0.45 eV/atom, respectively. The identical T_c for these two compositions is attributed to their shared $P\bar{1}$ symmetry and similar atomic arrangements. The $Zr_{0.25}Ta_{0.75}$ composition mixes at a higher temperature of ~1000 K, with an energy difference of 0.61 eV/atom. A clear trend emerges where the energy difference decreases with increasing Ta concentration. This is consistent with the higher melting point of tantalum compared to zirconium, which suggests stronger inherent bond strength and greater thermal stability. Consequently, structures with higher tantalum content are predicted to maintain stability and operate effectively at elevated temperatures. The propensity for Zr and Ta to mix well is likely due to their similar chemical properties, including high melting points and corrosion resistance, which promote strong intermolecular interactions and solid solution formation.

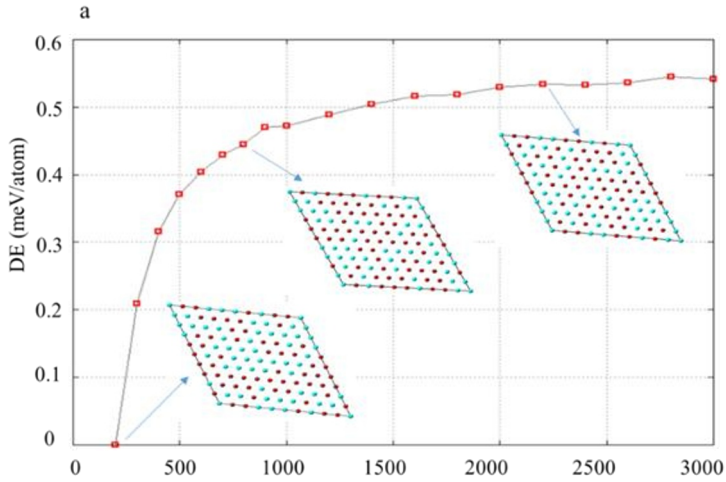

Fig. 3.1. Temperature-dependent energy profile for various Ta concentrations. The system with the lowest energy (most stable) is $Li_5La_3ZrTaO_{12}$ (space group P1).

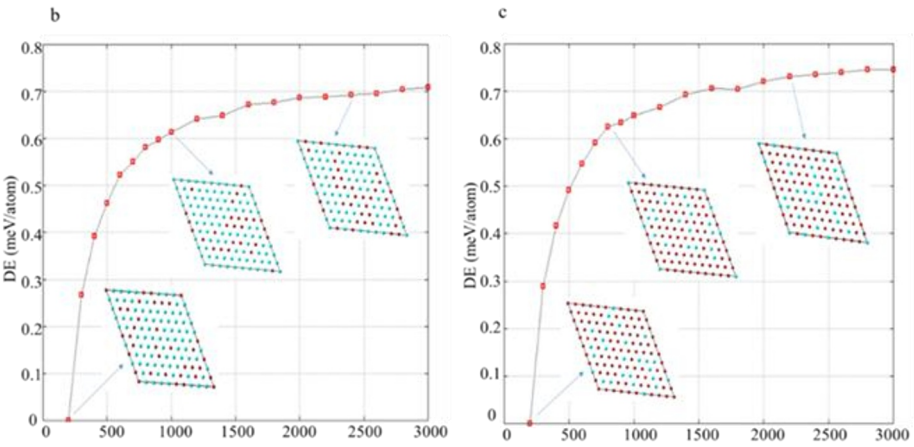

Fig. 3.2. Profiles are shown for **(a)** the most stable configuration, $Li_5La_3ZrTaO_{12}$ (P1); **(b)** a moderately Ta-doped system, $Li_5La_3Zr_{0.5}Ta_{1.5}O_{12}$ (C2/c); and **(c)** a moderately Zr-rich system, $Li_5La_3Zr_{1.5}Ta_{0.5}O_{12}$ (C2/c). The simulations track the evolution of free energy with temperature for each composition.

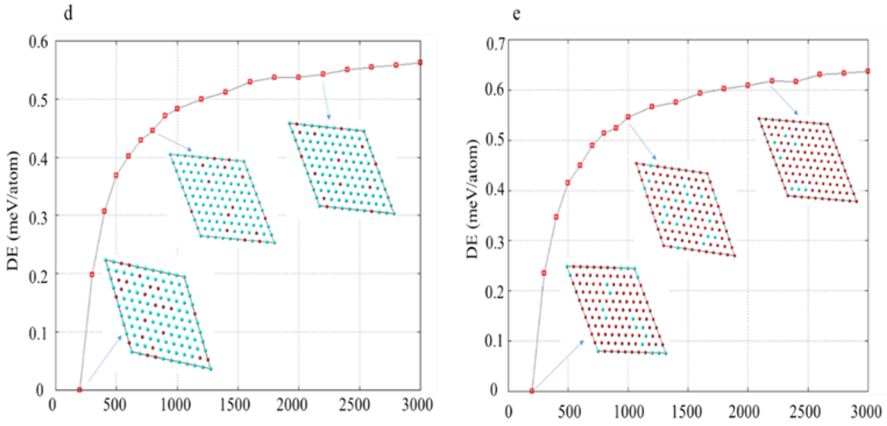

Fig. 3.3. Profiles are shown for **(d)** a highly Ta-rich composition, $Li_5La_3Zr_{0.25}Ta_{1.75}O_{12}$ (P1), and **(e)** a Zr-rich composition, $Li_5La_3Zr_{1.75}Ta_{0.25}O_{12}$ (P1). The data illustrate the thermodynamic stability of these endpoint-doped structures as a function of temperature.

4 Conclusion

In this work, first-principles cluster expansion (CE) calculations were employed to explore new phases of Ta-doped t-LLZO. The ground-state search revealed 28 thermodynamically stable multicomponent structures with negative enthalpies of formation, five of which were identified as the most stable, lying directly on the ground-state line. All generated structures exhibit a cross-validation score (CVS) below 5 meV, confirming the accuracy of the CE energy predictions and suggesting their practical applicability. Monte Carlo (MC) simulations further demonstrated excellent mixing behaviour at specific Ta doping concentrations ($Zr_{0.5}Ta_{0.5}$, $Zr_{0.25}Ta_{0.75}$ and $Zr_{0.125}Ta_{0.875}$) and temperatures (800 K, 1000 K, and 800 K, respectively). The systems showed no phase separation, with minimal energy differences (0.9 eV/atom, 0.61 eV/atom, and 0.45 eV/atom), indicating a homogeneous distribution of Ta in the LLZO matrix. These findings provide fundamental insights into the

phase stability of Ta-doped t-LLZO, supporting Zr-site doping as an effective strategy for optimizing LLZO-based solid-state electrolytes. This study lays the groundwork for future investigations into Li^+ diffusion kinetics and high-temperature ion mobility in these materials.

Acknowledgments The calculations were performed at the Materials Modelling Centre (MMC) at the University of Limpopo and the Centre for High Performance Computing (CHPC) in Cape Town. The authors also acknowledge the National Research Foundation (NRF) for their financial support. Furthermore, the support from the Advanced Materials Initiative (AMI) and MINTEK is highly appreciated.

Data availability : Data reported in this paper are available upon request to the corresponding author.

References

[1] P. Nzereogu, A. Oyesanya, S. Ogba, S. Ayanwunmi and et *al.,* Solid-State lithium-ion battery electrolytes: Revolutionizing energy density and safety. *Hybrid Adv.,* **8**, 100339, (2025). https://doi.org/10.1016/j.hybadv.2024.100339

[2] W. Zhao, J. Yi, P. He, and H. Zhou, Solid-State Electrolytes for Lithium-Ion Batteries: Fundamentals, Challenges and Perspectives. *Springer.,* **2**, 574–605, (2019). https://doi.org/10.1007/s41918-019-00048-0

[3] R. Maphoto, M. Masedi, P. Ngoepe, and R. Ledwaba, First-principles study on structural, mechanical and electronic properties of Li7La3Zr2O. *S. Afr. J. Sci..,* **40**, 12-15, (2021). https://doi.org/10.36303/SATNT.2021cosaami.03

[4] Y. M. Lee, J. E. Seo, N.-S. Choi, and J.-K. Park, Influence of tris(pentafluorophenyl) borane as an anion receptor on ionic conductivity of $LiClO_4$-based electrolyte for lithium batteries. *Electrochim. Acta,* **50**, 2843–2848, (2005). https://doi.org/10.1016/j.electacta.2004.11.058

[5] M. L. Lehmann, G. Yang, D. Gilmer, K. S. Han, E. C., Self, R. E. Ruther, et al., Tailored crosslinking of Poly(ethylene oxide) enables mechanical robustness and improved sodium-ion conductivity. *Energy Stor. Mater.,* **21**, 85–96, (2019). https://doi.org/10.1016/j.ensm.2019.06.028

[6] N. Janani, C. Deviannapoorani, L. Dhivya, and R. Murugan, Influence of sintering additives on densification and Li^+ conductivity of Al doped $Li_7La_3Zr_2O_{12}$ lithium garnet. *RSC Adv.,* **4**, 51228-51238, (2014). https://doi.org/10.1039/C4RA08674K

[7] L. Dhivya, K. Karthik, S. Ramakumar, and R. Murugan, Facile synthesis of high lithium ion conductive cubic phase lithium garnets for electrochemical energy storage devices. *RSC Adv.,* **5**, 96042-96051, (2015). https://doi.org/10.1039/C5RA18543B

[8] H. El Shinawi and J. Janek, Stabilization of cubic lithium-stuffed garnets of the type "$Li_7La_3Zr_2O_{12}$" by addition of gallium. *J. Power Sources,* **225**, 13-19, (2013). https://doi.org/10.1016/j.jpowsour.2012.09.111

[9] J. Wolfenstine, J. Ratchford, E. Rangasamy, J. Sakamoto, and J. L. Allen, Synthesis and high Li-ion conductivity of Ga-stabilized cubic $Li_7La_3Zr_2O_{12}$. *Mater. Chem. Phys.,* **134**, 571-575, (2012). https://doi.org/10.1016/j.matchemphys.2012.03.054

[10] Y. Zhang, F. Chen, and J. Li, Regulation mechanism of bottleneck size on Li^+ migration activation energy in garnet-type $Li_7La_3Zr_2O_{12}$. *Electrochim Acta.,* **261**, 137-142, (2018). https://doi.org/10.1016/j.electacta.2017.12.133

[11] J. Wolfenstine, E. Rangasamy, J. L. Allen, and J. Sakamoto, High conductivity of dense tetragonal $Li_7La_3Zr_2O_{12}$. *J. Power Sources,* **208**, 193-196, (2012). https://doi.org/10.1016/j.jpowsour.2012.02.031

[12] A. Düvel, and A. Kuhn, Mechanosynthesis of Solid Electrolytes: Preparation, Characterization, and Li Ion Transport Properties of Garnet-Type Al-Doped $Li_7La_3Zr_2O_{12}$ Crystallizing with Cubic Symmetry. *J Phys Chem C.,* **116**, 15192-15202, (2012). https://doi.org/10.1021/jp301193r

[13] M. R. Bonilla, F. A. Garcia-Daze, J. Carrasco, and E. Akhmatskaya, Exploring Li-ion conductivity in cubic, tetragonal and mixed-phase Al-substituted $Li_7La_3Zr_2O_{12}$ using atomistic simulations and effective medium theory. *Acta Mater.,* **175**, 426 (2019). https://doi.org/10.1016/j.actamat.2019.06.033

[14] A. Mark, D. de Fontaine, M. van Schilfgaarde, M. Sluiter, and M. Methfessel, First-principles phase-stability study of fcc alloys in the Ti-Al system. *Phys. Rev. B,* **46**, 5055, (1992). https://doi.org/10.1103/PhysRevB.46.5055

[15] M. Asta, R. McCormack, and D. de Fontaine, Theoretical study of alloy phase stability in the Cd-Mg system. (1993), *Phys. Rev. B*. **48**, 748. https://doi.org/10.1103/PhysRevB.48.748

[16] D. Lerch, O. Wiekhorst, G. L. W. Hart, R. W. Forcade, and S. Muller, UNCLE: a code for constructing cluster expansions for arbitrary lattices with minimal user-input. *Modelling Simul. Mater. Sci. Eng.,* **17**, 330, (2009). https://doi.org/10.1088/0965-0393/17/5/055003

[17] S. C. Abrahams and J. L. Bernstein, Rutile: Normal Probability Plot Analysis and Accurate Measurement of Crystal Structure**.** *J. Chem. Phys.,* **55**, 3206 – 3211, (1971). https://doi.org/10.1063/1.1676569

[18] J. P. Perdew and Y. Wang, Accurate and simple analytic representation of the electron-gas correlation energy**.** *Phys. Rev. B,* **45**, 13244, (1992). https://doi.org/10.1103/PhysRevB.45.13244